The University of Nottingham
UNITED KINGDOM · CHINA · MALAYSIA

Fischer, Sabine and Houston, Paul and Monk, Nick A.M. and Owen, Markus R. Is a persistent global bias necessary for the establishment of planar cell polarity? PLoS Computational Biology . ISSN 1553-734X (Submitted)

Access from the University of Nottingham repository:
http://eprints.nottingham.ac.uk/1696/1/Fischer_globalBias_PCP.pdf

Copyright and reuse:

The Nottingham ePrints service makes this work by researchers of the University of Nottingham available open access under the following conditions.

This article is made available under the University of Nottingham End User licence and may be reused according to the conditions of the licence. For more details see: http://eprints.nottingham.ac.uk/end_user_agreement.pdf

A note on versions:

The version presented here may differ from the published version or from the version of record. If you wish to cite this item you are advised to consult the publisher's version. Please see the repository url above for details on accessing the published version and note that access may require a subscription.

For more information, please contact eprints@nottingham.ac.uk

Is a Persistent Global Bias Necessary for the Establishment of Planar Cell Polarity?

Sabine Fischer[1,2,*], Paul Houston[1], Nicholas A. M. Monk[1,3], Markus R. Owen[1]

1Centre for Mathematical Medicine and Biology, School of Mathematical Sciences, University of Nottingham, Nottingham, UK

2 current address: Buchmann Institute of Molecular Life Sciences, Institute of Biological Sceinces, Goethe University Frankfurt, Frankfurt am Main, Germany

3 current address: Centre for Membrane Interactions and Dynamics, School of Mathematics and Statistics, University of Sheffield, Sheffield, UK

∗ **E-mail: Sabine.Fischer@physikalischebiologie.de**

Abstract

Planar cell polarity (PCP) — the coordinated polarisation of a whole field of cells within the plane of a tissue — relies on the interaction of three modules: a global module that couples individual cellular polarity to the tissue axis, a local module that aligns the axis of polarisation of neighbouring cells, and a readout module that directs the correct outgrowth of PCP-regulated structures such as hairs and bristles. While much is known about the molecular components that are required for PCP, the functional details of—and interactions between—the modules remain unclear. In this work, we perform a mathematical analysis of two previously proposed computational models of the local module (Amonlirdviman et al., Science, 307, 2005; Le Garrec et al., Dev. Dyn., 235, 2006). Both models can reproduce wild-type and mutant phenotypes of PCP observed in the *Drosophila* wing under the assumption that a tissue-wide polarity cue from the global module persists throughout the development of PCP. We demonstrate that both models can also generate tissue-level PCP when provided with only a transient initial polarity cue. However, such transient cues are not sufficient to ensure robustness of the resulting cellular polarisation.

Author Summary

Cell polarisation is an important feature of development and is critical for many organ functions. A cell is polarised if it is possible to distinguish different ends, e.g., by shape or by an asymmetric protein distribution within the cell. The phenomenon of a whole field of cells that are coordinately polarised within the plane of the tissue is commonly referred to as planar cell polarity (PCP). Dysfunction of PCP pathways can lead to a wide range of diseases including congenital deafness syndromes and polycystic kidneys. The animal most studied in this context is the fruit fly *Drosophila*. We focus on the establishment of PCP in the wings, which is manifested by an alignment of hairs. In this work, we present an analysis of two models that have been proposed in recent years. Both models are based on feedback loops that read and amplify a global bias. We demonstrate that robust polarity over large areas of cells requires the bias to be maintained during the whole development of PCP in the wing, and show how the feedback loops influence the strength of polarisation.

Introduction

During embryonic development, the correct formation of tissues and organs requires coordinated rearrangements of cells, which rely on the polarisation of the cells along their apical-basal axis and in many epithelia also within the plane of the tissue. The latter is commonly referred to as planar cell polarity (PCP). Disruption of PCP significantly affects morphogenetic events such as gastrulation and neurulation [1] and impairs body functions such as polarised ciliary beating [2], leading to a variety of diseases including congenital deafness syndromes, neural tube closure defects, respiratory diseases and polycystic kidneys [3].

The fruit fly *Drosophila melanogaster* is an important model organism for studying the mechanism of PCP establishment, since it displays overt PCP features on all adult external structures. The most obvious examples of this are the orientation of the ommatidia in the eyes and the alignment of hairs on the wings and the abdomen. In all of these tissues, PCP is believed to be

controlled by interactions between three modules [4, 5]. A global module provides a tissue-wide directional cue that links cellular polarity to the tissue axis; a local module enables cells to align their polarity with their neighbours; and the third module performs the readout. Although the existence of these modules is commonly accepted, the molecular details of the global module are controversial and the interactions of the three modules remain unclear. Initially it was assumed that the three modules worked in a linear sequence: the global module would affect only the local module which would in turn provide the information for the readout. However, recent results point increasingly towards more complex network type interactions in which both the global and the local module directly affect the readout as well as each other.

To date, much emphasis has been placed on the local module, and a range of experimental evidence has revealed that a system of interacting proteins centred around the transmembrane protein Frizzled (Fz) plays a key role. This group of proteins — often referred to as core proteins — includes the atypical cadherin Flamingo (Fmi), the transmembrane protein Van Gogh (Vang; also known as Strabismus) and the cytoplasmic proteins Dishevelled (Dsh) and Prickle (Pk). During the establishment of PCP these five proteins acquire an asymmetric distribution within cells. In the *Drosophila* pupal wing, shortly before hair formation, Fz and Dsh become localised to the distal membrane of each cell, while Vang and Pk colocalise in the proximal membranes. Fmi occurs in both the proximal and the distal membrane, but not anterior or posterior [6]. Figure 1 shows an illustration of the protein distribution.

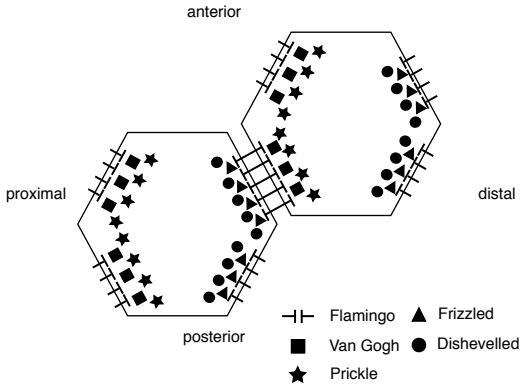

Figure 1. Localisation of the PCP core proteins at the cell edges.

While the identities of the key molecular species involved in the local module are well established, the way in which they interact to establish their overt patterns of asymmetric localisation is less clear. In recent years two computational models for the local module in the *Drosophila* wing have been proposed. These models incorporate distinct subsets of the core proteins and explore different proposals for their interactions [7,8]. A common feature of the two models is that the interactions between the core proteins are biased within each cell by a tissue-wide polarity cue from the global module. Importantly, this cue persists throughout the whole process of local cell polarisation, and is "read" and amplified by a feedback loop which consists of interactions between the core proteins. The two models differ in the type of persistent global bias and the details of their feedback mechanisms. Both models aim to reproduce the wild type asymmetric distribution of the core proteins, as shown in Figure 1, as well as the patterns around mosaic cell clones which lack or over-express one of the core proteins.

The ability of these models to produce patterns of PCP that mimic those observed experimentally raises an important question: what are the relative roles played by the persistent global polarity cue and by the local feedback amplification mechanism? An analysis of the models with respect to the wild type polarity will give insight into the relative importance of the persistent global bias and the feedback loop for the establishment of PCP, while focusing on the mutant conditions would address the differences between the feedback loops. In this work we are interested in the interplay of the global and the local module and therefore we consider the wild type situation. In the following we will introduce the two models in detail and analyse their capability of reproducing the wild type in one and two spatial dimensions. We find that, in these models, robust long-range coordination of polarity relies on the persistent global bias and the feedback mechanisms enhance the strength of polarity. In both cases, the global bias is only required to ensure robustness; to generate polarity a small initial imbalance in the cells is sufficient.

Models

In this work, we analyse the mechanisms proposed by Amonlirdviman *et al.* [7,9] and Le Garrec *et al.* [8] (applied to the eye in [10]). Both have a common general structure consisting of a persistent imposed global bias which is amplified by a feedback mechanism, that is based on protein complex formation. To globally bias the polarity of the cells Amonlirdviman *et al.* consider two different mechanisms, a cell intrinsic polarity in the dissociation rates for certain complexes and a polarity for the diffusion of certain proteins and complexes [7]. They find that both versions of their model give similar results. In Le Garrec *et al.* the global module is introduced by appling a ligand gradient over the whole tissue [8]. For the feedback mechanism the two approaches include different members of the core proteins and assume different interactions as described below.

Model A

This model is based on the mechanism proposed by Amonlirdviman *et al.* [7], which includes the protein interactions illustrated in Figure 2.

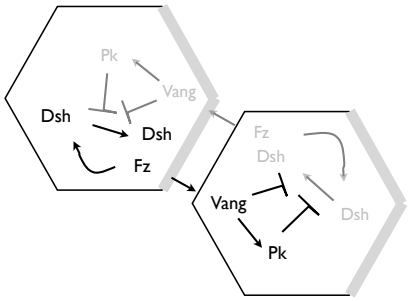

Figure 2. Feedback loop and global bias of Model A. The amounts of proteins in black are higher than the amounts of proteins in grey. Arrows represent recruitment of proteins, T-signs inhibition. The grey regions at the distal sides of the cell indicate where the persistent global bias affects the dissociation rate of Dsh. This figure was reproduced from Fig 2B in [7].

Assuming that the proteins colocalise by forming complexes, the model can be summarised

by the following reactions.

$$Dsh + Fz \underset{AB\lambda_1}{\overset{R_1}{\rightleftharpoons}} DshFz, \tag{1}$$

$$Fz^+ + Vang \underset{\lambda_2}{\overset{R_2}{\rightleftharpoons}} Fz = Vang, \tag{2}$$

$$Vang + Pk \underset{\lambda_3}{\overset{R_3}{\rightleftharpoons}} VangPk, \tag{3}$$

$$DshFz^+ + Vang \underset{\lambda_4}{\overset{R_4}{\rightleftharpoons}} DshFz = Vang, \tag{4}$$

$$Dsh^+ + Fz = Vang \underset{A^+B^+\lambda_5}{\overset{R_5}{\rightleftharpoons}} DshFz = Vang, \tag{5}$$

$$Fz^+ + VangPk \underset{\lambda_6}{\overset{R_6}{\rightleftharpoons}} Fz = VangPk, \tag{6}$$

$$Fz = Vang + Pk \underset{\lambda_7}{\overset{R_7}{\rightleftharpoons}} Fz = VangPk, \tag{7}$$

$$Dsh^+ + Fz = VangPk \underset{A^+B^+\lambda_8}{\overset{R_8}{\rightleftharpoons}} DshFz = VangPk, \tag{8}$$

$$DshFz^+ + VangPk \underset{\lambda_9}{\overset{R_9}{\rightleftharpoons}} DshFz = VangPk, \tag{9}$$

$$DshFz = Vang + Pk \underset{\lambda_{10}}{\overset{R_{10}}{\rightleftharpoons}} DshFz = VangPk. \tag{10}$$

For each equation i with $i = 1, \ldots, 10$, there is a forward reaction rate R_i and a backward reaction rate λ_i. The superscript $^+$ emphasises that the two reactants are in different cells, binding over the cell membrane to form a cell bridging complex which is indicated by $=$. We adopt the notation that the cell bridging complexes belong to the same cell as their Vang part. The different proteins and complexes have different regions in which they can move. Dsh and Pk can be found in the cytoplasm. Fz, Dsh, DshFz and VangPk can move along the whole membrane of a cell, while the cell bridging complexes are restricted to the part of the membrane that is common to the two cells they connect.

Out of the two mechanisms Amonlirdviman *et al.* proposed for their persistent global bias, we have implemented the bias in dissociation rates. Thereby, the rates of dissociation of Dsh from Dsh-containing complexes in a region of the distal side of each cell are decreased by multiplying

the backward reaction rates of equations (1),(5) and (8) by a factor $A \leq 1$ whith

$$A = \begin{cases} M_1, & \text{distal region of the cell,} \\ 1, & \text{otherwise,} \end{cases}$$

and $M_1 < 1$. In [9] the persistent global bias was refined from a step function to an intracellular gradient, allowing different directions of the bias in clones that are assumed to interfere with the global module. However, for the purpose of this paper it is sufficient to consider the stepwise global bias along the proximal-distal axis of a cell.

The amplification of this imposed polarity by the local module is achieved in this model by a feedback loop, that consists of Vang and its complexes inhibiting the recruitment of Dsh to complexes. As shown in Figure 2 this inhibition occurs within the same cell. This implies that if we have Vang or its complexes in a given cell, the recruitment of Dsh in that same cell is inhibited, not the recruitment of Dsh from the neighbouring cell to this Vang-complex.

In the equations the feedback is represented by an increase of the backward reaction rates of all the reactions in which Dsh binds to Fz or Fz complexes, namely reactions (1), (5) and (8). To this end, those backward reaction rates are multiplied by a factor $B \geq 1$ with

$$\begin{aligned} B = 1 + K_b(K_{pk}[Pk] + [VangPk] + [FzVangPk] + [DshFzVangPk] \\ + K_{va}([Vang] + [FzVang] + [DshFzVang]))^{K_p}, \end{aligned}$$

where K_b, K_{pk}, K_{va} and K_p are positive constants. We see that B is an increasing function of the concentrations of Pk, Vang and their complexes in the same cell as Dsh.

We are interested specifically in the relative importance of the persistent global bias and the feedback loop in this model for the establishment of PCP. To this end, we analyse two discretisations of the model and conduct simulations of the full spatial system. In our one-dimensional discretisation we assume each cell has two sides, left and right, with certain amounts of the protein and protein complexes, a representation we have previously applied in [11]. In this setting, diffusion is implemented as exchange between the two sides of the cell. This approach enables us to deter-

mine which parameter combinations yield polarity, and which yield a homogeneous unpolarised steady state in the one-dimensional model. The two-dimensional discretisation assumes that each cell is hexagonal and consists of six compartments and that intracellular diffusion occurs between neighbouring compartments. This two-dimensional version of the model introduces the possibility of different types of polarisation, towards either a side or a vertex of a cell (see Results section). In the supplementary section we discuss the results from the simulations of the full spatial model, for which we assume that each cell is a continuous hexagon. We performed these simulations to ensure that our results on simplified geometries are not artefacts of the discretisation.

The systems of differential equations corresponding to the different versions of Model A are obtained from the reactions (1)–(10) by applying the law of mass action and linear diffusion of mobile components between neighbouring cellular compartments. Example equations can be found in the supplementary material.

Model L

Model L incorporates the mechanism proposed by Le Garrec *et al.* in [8]. In this model, the global bias is provided by an initial tissue-wide ligand gradient, while the local amplification module relies on the feedback loops summarised in Figure 3. The interactions of the proteins and protein complexes can be described by the following reactions:

$$Fz + Ld \xrightarrow{Kf_1} Fz^*, \tag{11}$$

$$Fz^* + Fmi \underset{Kd_2}{\overset{Kf_2}{\rightleftharpoons}} Fz^*Fmi, \tag{12}$$

$$Vang + Fmi \underset{en3\ Kd_3}{\overset{inh3\ Kf_3}{\rightleftharpoons}} FmiVang, \tag{13}$$

$$Fz^*Fmi + FmiVang \underset{Kd_4}{\overset{Kf_4}{\rightleftharpoons}} Fz^*Fmi = FmiVang, \tag{14}$$

$$Fz^*Fmi = FmiVang + Pk \quad \underset{en5\ Kd_5}{\overset{inh5\ Kf_5}{\rightleftharpoons}} \quad Fz^*Fmi = FmiVangPk, \tag{15}$$

$$Dsh + Fz^*Fmi = FmiVang \quad \underset{Kd_6}{\overset{Kf_6}{\rightleftharpoons}} \quad Dsh^*FzFmi = FmiVang, \tag{16}$$

$$Dsh + Fz^*Fmi = FmiVangPk \quad \underset{Kd_7}{\overset{Kf_7}{\rightleftharpoons}} \quad Dsh^*FzFmi = FmiVangPk, \tag{17}$$

$$Dsh^*FzFmi = FmiVang + Pk \quad \underset{en8\ Kd_8}{\overset{inh8\ Kf_8}{\rightleftharpoons}} \quad Dsh^*FzFmi = FmiVangPk. \tag{18}$$

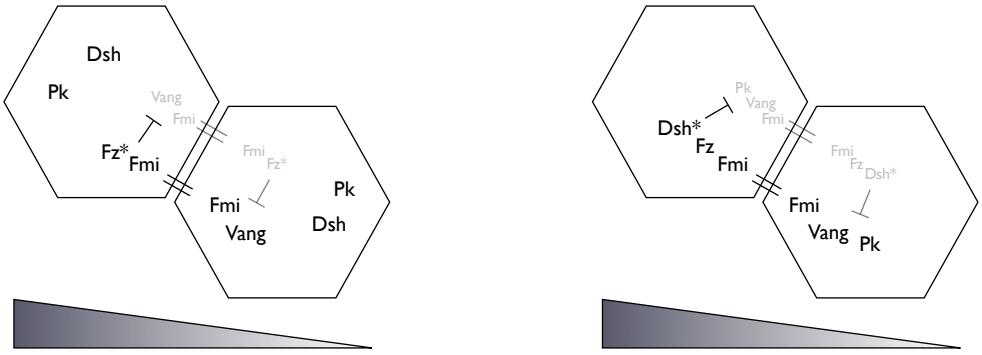

(a) (b)

Figure 3. Feedback mechanism and global bias of Model L. Light grey represents a smaller protein concentration than black. Binding over the cell membrane is indicated by = and T means inhibition. (a) First feedback loop: Fz* and its complexes inhibit the binding of Vang to Fmi, (b) second feedback loop: the Dsh* complexes inhibit the binding of Pk to Vang complexes (Dsh is phosphorylated when binding to the Fz*-ends of the cell bridging complexes, becoming Dsh*). The triangles at the bottom represent the tissue-scale ligand gradient.

Ld represents a hypothetical ligand that binds to Fz, and Fz^* denotes the bound (or ligand-activated) form of Fz. Dsh becomes phosphorylated on binding to the Fz*-ends of the cell bridging complexes, and is then denoted by Dsh^*. The symbol = indicates complexes that bridge the membranes of two neighbouring cells. The forward reaction rates are Kf_i and the backward reaction rates are Kd_i with $i = 1, \ldots, 8$. The two feedback loops are implemented by decreasing the forward reaction rates and increasing the backward reaction rates of equation (13) in response to the concentration of Fz* and Fz* complexes, and equations (15) and (18) in

response to the concentration of Dsh* complexes. The factors are

$$inh3 = \frac{1}{1 + A_3([Fz^*] + [Fz^*Fmi] + [Fz^*FmiFmiVang] + [Fz^*FmiFmiVangPk])},$$
$$inh5 = \frac{1}{1 + A_5([Dsh^*FzFmiFmiVang] + [Dsh^*FzFmiFmiVangPk])},$$
$$inh8 = \frac{1}{1 + A_8([Dsh^*FzFmiFmiVang] + [Dsh^*FzFmiFmiVangPk])},$$

and

$$en3 = 1 + B_3([Fz^*] + [Fz^*Fmi] + [Fz^*FmiFmiVang] + [Fz^*FmiFmiVangPk]),$$
$$en5 = 1 + B_5([Dsh^*FzFmiFmiVang] + [Dsh^*FzFmiFmiVangPk]),$$
$$en8 = 1 + B_8([Dsh^*FzFmiFmiVang] + [Dsh^*FzFmiFmiVangPk]),$$

where A_i and B_i $(i = 3, 5, 8)$ are positive constants.

As outlined above for Model A, we analyse this model for a one-dimensional and a two-dimensional discretisation and conduct simulations of the full spatial model. The systems of differential equations corresponding to reactions (11)–(18) are obtained by applying the law of mass action and linear diffusion of mobile proteins between neighbouring cellular compartments. The supplementary material contains sample equations for each case.

Results

Amonlirdviman *et al.* and Le Garrec *et al.* showed that their respective mechanisms, Model A and Model L are capable of polarising a whole field of cells simultaneously. In both cases the results are based on numerical simulations of fields of two-dimensional hexagonal cells. The models have a common logical structure in that both consist of feedback mechanisms amplifying an imposed global bias. However, the relative importance of these two components (imposed

bias and local feedback) for the generation of coherent tissue-wide patterns of PCP is unclear. We addressed this issue by analysing the two models. Since the full models in two spatial dimensions are rather complex and do not lend themselves to analysis very easily, we initially reduced the models to one spatial dimension.

Model A: Both persistent global bias and feedback can generate polarity independently

To represent the tissue in one spatial dimension we considered a line of two-sided cells. On each side of a cell there are certain concentrations of the four proteins Dsh, Fz, Vang and Pk, with intracellular diffusion between the two sides of a cell. We simulated the model in Matlab for a row of ten cells with periodic boundary conditions and the parameter values in Table S1. As the readout, we present the final distributions of total Dsh and total Vang in each cell, which in each case include all relevant complexes.

We started our analysis by investigating the ability of the persistent imposed global bias to determine the final distributions of total Dsh and total Vang as shown in Figure 4. For the initial conditions (shown in Figure 4(a)) we used a strong global polarity for Dsh and Vang, opposite to the normal wild type distribution presented in Figure 1. Pk and Fz are initially distributed homogeneously in every cell, and there are no complexes. This type of initial condition is used to emphasise the effect of the persistent global bias.

The persistent global bias is represented by the parameter M_1, such that $0 < M_1 < 1$, with lower values of M_1 corresponding to a stronger bias (for more details see the Models section and the supplementary material). Figure 4(b) shows the final state for $M_1 = 0.2$. The polarity of the final state is reversed compared to the polarity of the initial conditions. Weaker global bias (larger values of M_1) yields weaker polarity, but in the same direction (not shown). To compare these results with a final state that relies only on the persistent global bias we performed the simulation with the same initial condition and the same strength of the global bias but with the feedback loop switched off. This yields a weaker polarity (Figure 4(c)) but its direction is still reversed compared to the direction of the initial condition in Figure 4(a). Thus, the persistent

global bias has a very strong impact on the final polarity, since it can override the direction of polarity of the initial conditions.

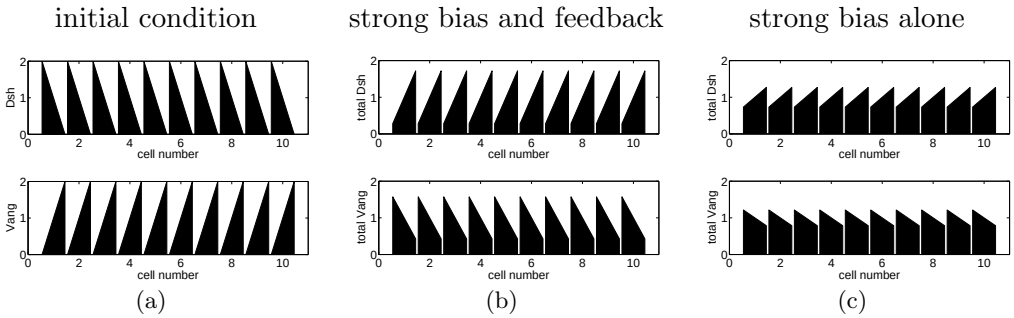

Figure 4. The persistent global bias has a strong impact on the final states of Model A. (a) initial condition with a strong polarity of Dsh and Vang in the direction opposite to the direction of the final state observed in experiments. Pk and Fz are initially distributed homogeneously; (b) final state for $M_1 = 0.2$ and the parameter values in Table S1; (c) final state for a global bias of $M_1 = 0.2$, the parameter values in Table S1 but with no feedback (i.e. $K_b = 0$).

As a next step we considered the behaviour of the system if there is no persistent global bias, which corresponds to $M_1 = 1$. Figure 5 shows the results for different strengths of feedback. In this case, we considered a biologically motivated small initial distal (right) imbalance in Fz distribution in every cell as shown in Figure 5(a). Initially, the other proteins are distributed homogeneously. The corresponding results are displayed in Figure 5(b)-(d). They demonstrate that an imposed global bias is not required for the generation of polarity, if the feedback is sufficiently strong (Figure 5 (b), (c)). A stronger feedback yields a stronger polarity of the final state as shown in Figure 5(c). To analyse the impact of the initial imbalance on the final polarity, we varied its strength from -0.2 (imbalance to the left) to 0.2 (imbalance to the right). We found that a small initial imbalance is necessary to break symmetry, and that the direction of the polarity of the final state depends on the direction of the imbalance in the initial conditions (Figure 6). These results show that the feedback mechanism alone can generate bistability across the membranes of two neighbouring cells, and thereby amplify small initial imbalances in protein distribution to generate strong cellular polarity. Without the imposition of persistent global bias, this model provides a specific example of the conservative model class described

in [11].

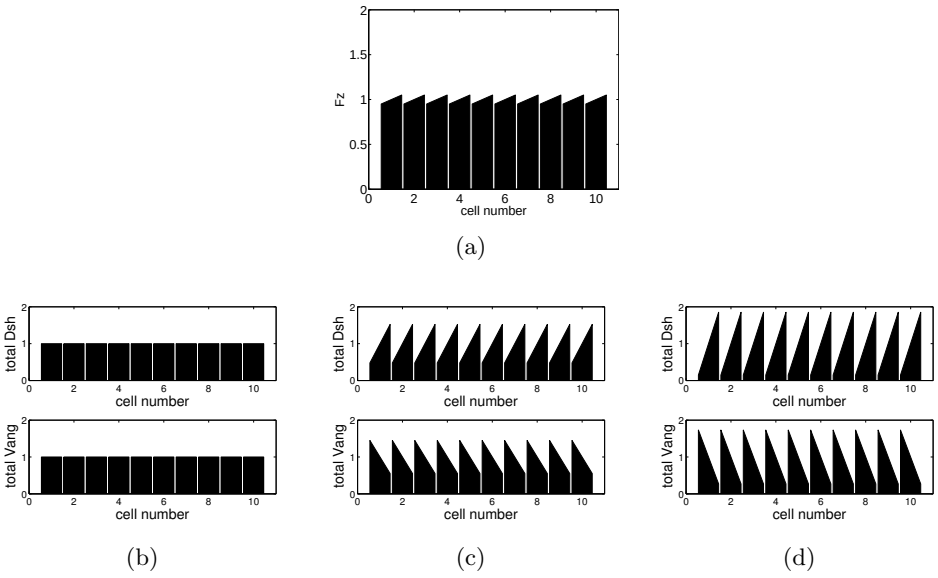

Figure 5. Final states of Model A for different strengths of feedback with no imposed global bias. (a) Initial condition: an imbalance in Fz with a difference of 0.1 between right and left side; initially, the other proteins are distributed homogeneously; (b) final distribution of total Dsh and total Vang for a weak feedback with the corresponding parameter values $K_b = 10$ and $K_p = 1.9$, (c) final distribution of total Dsh and total Vang for a stronger feedback with $K_b = 10$ and $K_p = 2.2$, (c) final distribution of total Dsh and total Vang for an even stronger feedback with $K_b = 20$ and $K_p = 5$. All other parameter values as listed in Table S1.

Our results for the one-dimensional discretisation show that with an imposed persistent global bias, Model A generates polarity in the direction of the bias irrespective of the initial conditions and the feedback loop. In the absence of an imposed global bias, a small initial imbalance in protein distribution in each cell is necessary to initiate polarisation. In this case, the direction of the polarity depends on the direction of the initial imbalance while the strength of the polarity depends on the strength of the feedback. Without either an initial protein imbalance or an imposed global bias, all cells remain unpolarised.

Model L: The imposed ligand gradient determines both the strength and direction of polarity

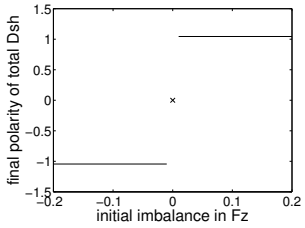

Figure 6. Effect of the initial Fz imbalance in Model A with no imposed global bias. We consider a row of ten cells with identical initial conditions. The strength of the initial imbalance in Fz is determined by the difference in Fz between the right and left sides of a cell; the other proteins are initially distributed homogeneously. The strength of the final polarity is given as the difference in total Dsh between the right and left sides of a cell. The parameter values are shown in Table S1.

Le Garrec *et al.* used a stochastic approach for the simulations of their model. To simplify the analysis, and to make the results comparable to those for Model A in the previous section and to our results for general classes of models in [11], we used instead a deterministic approach. As in the previous section, we assumed a row of two-sided cells with certain concentrations of the six proteins and complexes on each cell side. To ensure that our modified version of the model gives similar results to the original one we commenced our analysis by simulating the model in Matlab for the initial ligand gradient and the parameter values given in [8], adapted to the geometry in our simulations (supplementary material). We chose the concentrations of the proteins in each membrane pixel in [8] as our initial protein concentrations. Hence, initially Fz, Fmi, Vang, Dsh and Pk are distributed homogeneously in every cell, with $[Fz]_i^l = [Fz]_i^r = 4, [Fmi]_i^l = [Fmi]_i^r = 4, [Vang]_i^l = [Vang]_i^r = 2, [Dsh]_i^l = [Dsh]_i^r = 2$ and $[Pk]_i^l = [Pk]_i^r = 2$ for all cells i. As boundary conditions we assumed that at both ends of the row we have boundary cells (cells 1 and N) in which $c_1^l = 0, c_1^r = c_2^l, c_N^l = c_{N-1}^r$ and $c_N^r = 0$, where c_i^l and c_i^r are the concentrations of any protein or protein complex in cell i on the left and right side, respectively. Furthermore, all intracellular diffusion coefficients in cell 1 and cell N are zero; the remaining interactions in these cells are governed by the same equations as for the rest of the cells. In [8] there are roughly 13 cells in each row. Therefore, we simulated the system for 11 cells plus 2 boundary cells. Figure 7 shows the corresponding results. We present

the final distribution of the sum of the Dsh* complexes, since in [8] this is assumed to determine the direction of the hair growth; the hairs are assumed to grow at the end of the cell with the highest Dsh* concentration. We see that our modified version of the model gives similar results to the original model in [8], in that we obtain polarity to the right in every cell. Due to the boundary conditions, the polarity of the cells at the two ends of the row is weaker than that of cells in the middle of the row.

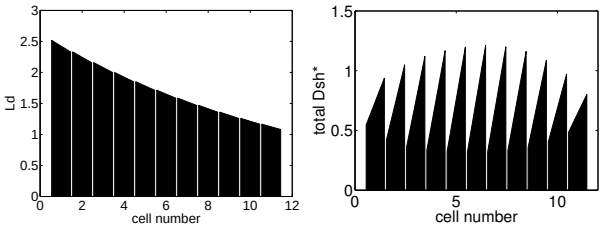

(a) (b)

Figure 7. Model L gives similar result to the original model in [8]. (a) Initial imposed ligand gradient from [8], adopted to our geometry; (b) final Dsh* distribution from a deterministic simulation for the parameter values in [8](see Table S4). The weaker polarity in the first and last cell of the row is due to the boundary conditions.

To gain more insight into the effect of the initial ligand gradient we choose the different gradients shown in Figure 8 A1-A4 and compare the corresponding final Dsh* distributions. In Figure 8 A1 we assume a decreasing linear ligand gradient. We see in B1 that this initial gradient yields a similar final state to the exponential gradient in Figure 7(a). The same is true for an initial condition in which the initial amount of ligand is the same on both sides of each cell (not shown).

Investigating other properties of the initial ligand gradient we find that its direction determines the direction of polarity. An increasing gradient leads to polarity to the left (not shown). The strength of polarity is affected by the slope of the gradient such that a shallower gradient yields weaker polarity as shown in Figure 8 column 2. The amount of Ld in a cell is also important. In A2 the total amount of Ld in each cell is higher than for Vang, Dsh or Pk. If we choose the initial ligand gradient such that there is less Ld in each cell than any of the other proteins, we

get stronger polarity. This is shown in Figure 8, column 3 where the initial gradient in A3 has the same slope as the gradient in A2 but lower levels of Ld. Column 4 shows the initial ligand gradient alone is sufficient to generate polarity — the initial gradient in A4 is the same as in A1 and B4 shows the results if there is no feedback.

These results demonstrate that both the slope and the total amounts of Ld in the initial gradient determine the strength of polarity and the direction of polarity depends on the direction of the gradient. Furthermore, to establish polarity the initial gradient is sufficient, however the feedback loops enhance the strength of polarity.

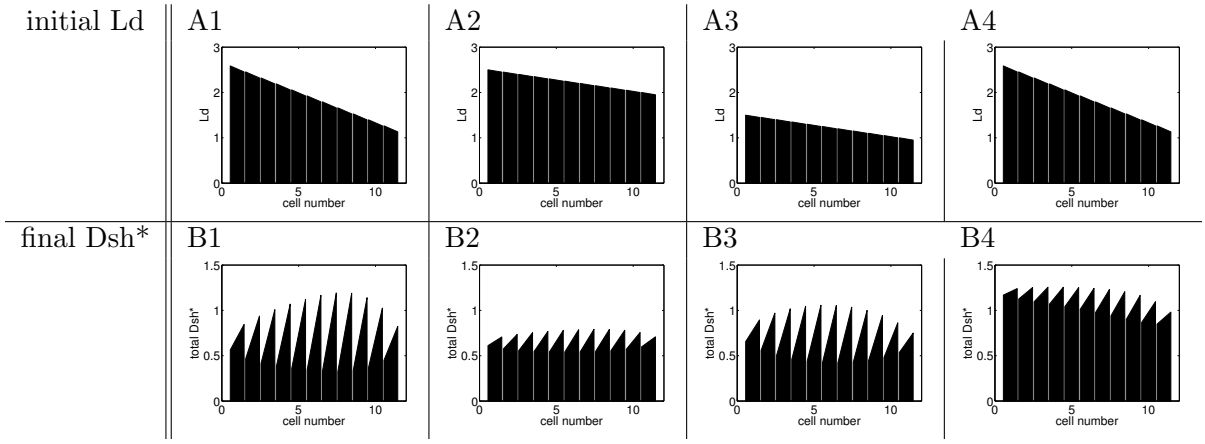

Figure 8. Different initial ligand gradients and the corresponding final Dsh* distributions for Model L. Column 1: The weaker polarity in the first and the last cell of the row is due to the boundary conditions. The polarity in the left half of the row is weaker because in cells 1–3 there is more ligand than Dsh, Vang and Pk; column 2: a shallow gradient with high levels of Ld gives weak polarity; column 3: for a shallow gradient with lower levels of Ld we get stronger polarity; column 4: the same initial gradient as in A1 and no feedback ($A_3 = A_5 = A_8 = B_3 = B_5 = B_8 = 0$) yields weaker polarity than in B1.
The parameter values are shown in Table S4.

Our results show that the initial gradient has a similar effect to the persistent global bias in Model A; it gives the system a bias that lasts for the whole process, preventing any homogeneous unpolarised steady states. Therefore, our next aim was to investigate whether an initial ligand distribution without a tissue-scale gradient, but rather with a small imbalance in every cell, can also yield polarity. The initial condition and the corresponding final state for a row of ten

cells are shown in Figure 9. Note that we chose a different set of parameter values because we found that for the parameter values used in [8] the cells did not polarise autonomously (see supplementary material). The total amount of ligand in each cell is less than the total amount of any other protein to ensure that we do not get weaker polarity caused by excessive amounts of Ld as observed above (Figure 8). Here, we applied periodic boundary conditions; our simulations represent an infinite line of cells and the results do not depend on the number of cells chosen. Figure 9 shows that we get strong polarity. We further analysed the effect of the initial imbalance on the final distribution of total Dsh*. We find that the direction and the strength of polarity depends on the direction and strength of the initial ligand imbalance as shown in Figure 10. Without an initial imbalance we do not get polarity. Hence, provided an initial imbalance, the feedback mechanism can generate a bistability across the membrane and the system of feedback mechanisms of this model is another example of the general conservative model class discussed in [11].

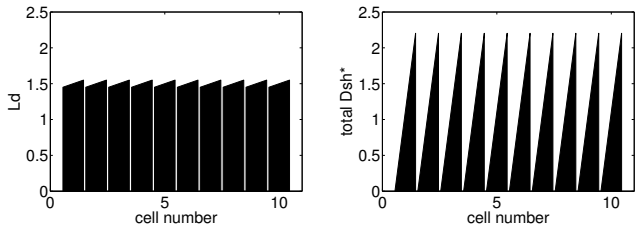

Figure 9. For a small initial imbalance in each cell Model L can yield polarity (a) Initial ligand distribution with a small imbalance in every cell, the difference between left and right in each cell is 0.1. Initially, the other proteins are distributed homogeneously and there are no protein complexes. (b) Final state of total Dsh* for the parameter set in Table S5.

Our analysis has shown that, in both models, the global cue ensures polarity and determines its direction, while the feedback mechanism controls the strength of the polarisation. In the absence of the global cue the feedback mechanism can yield an unpolarised state or polarity depending on the parameter values and the initial condition. For certain parameter values a small initial imbalance is amplified and the direction of polarity depends on the direction of the initial condition. As a next step we were interested to determine the extent to which this

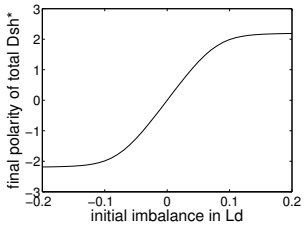

Figure 10. Effect of the initial imbalance on the final polarity of Model L. We consider a row of 10 cells with identical initial conditions. The difference in Ld between right and left side of a cell determines the strength of the initial imbalance; initially, the other proteins are distributed homogeneously. The strength of the final polarity is given as the difference in total Dsh* between right and left side of a cell. We used the parameter values in Table S5.

result is valid for hexagonal cells. While in two sided cells in one spatial dimension there is only one type of inhomogeneous steady state, in two spatial dimensions with hexagonal cells we have to distinguish between vertex polarity, side polarity and a triangular state as illustrated in Figure 11. Since in the wild type *Drosophila* wing the hairs grow from the most distal tip of approximately hexagonal cells, we are mainly interested in vertex polarity (Figure 11(b)). In the next section, we extend our analysis of the two models to hexagonal cells in two spatial dimensions. The persistent global cues yield only vertex polarity, since they impose symmetry constraints which are inconsistent with side polarity and the triangular states. Therefore, we omit global cues and investigate which steady states the feedback mechanisms alone can generate and whether they are stable.

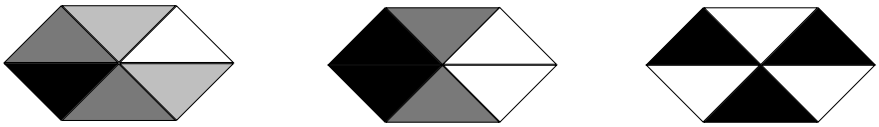

(a) (b) (c)

Figure 11. In two spatial dimensions three different types of inhomogeneous steady states can occur: (a) a side polarised configuration, (b) a vertex polarised configuration; (a, b) both polarisations are possible in six directions, (c) a triangular state.

Without the global bias vertex polarity is unstable

First, we focus on Model A, omitting the persistent global bias. We assume hexagonal cells, which are divided into six compartments. Diffusion occurs between a compartment and its two neighbouring compartments in the same cell. Details about the system of equations are given in the supplementary material. Analysing the existence and stability of the steady states for our system with 60 equations per cell is very complex. Therefore, we conducted a numerical analysis. We simulated the system for one cell, applying periodic boundary conditions for the intercellular binding. Hence, our domain represents an infinite field of hexagonal cells with the same initial conditions. To determine the steady states of this system we chose random initial conditions and systematically varied the diffusion coefficients and the strength of the feedback (see Table S2). As a readout we used the distribution of total Dsh which is assumed to initiate hair formation in the *Drosophila* wing. For every steady state we found, we calculated the eigenvalues of the corresponding linearised system to determine its stability.

Depending on the parameter values, we find that either the unpolarised steady state, the side polarised state in one of the six directions or a triangular state is stable. A map of the results from the parameter scan and example steady states for the different types are shown in Figure 12 and 13. Within the range of our parameter scan intermediate feedback strength combined with weak intracellular diffusion yield the triangular state. For higher diffusion the system tends to a side polarised state and the direction of polarity depends on the direction of the initial condition. Increasing diffusion further yields the unpolarised state. The vertex polarised state does not occur in our parameter scan. Choosing an initial condition which has a slight vertex polarity, the system tends to a vertex polarised state for certain diffusion and feedback strengths, but these states are unstable.

For Model L we conducted a similar analysis. We assumed compartmentalised hexagonal cells and performed a parameter scan to determine the stable states of the system (Figure 14). Details about the corresponding system of equations and the parameter values can be found in

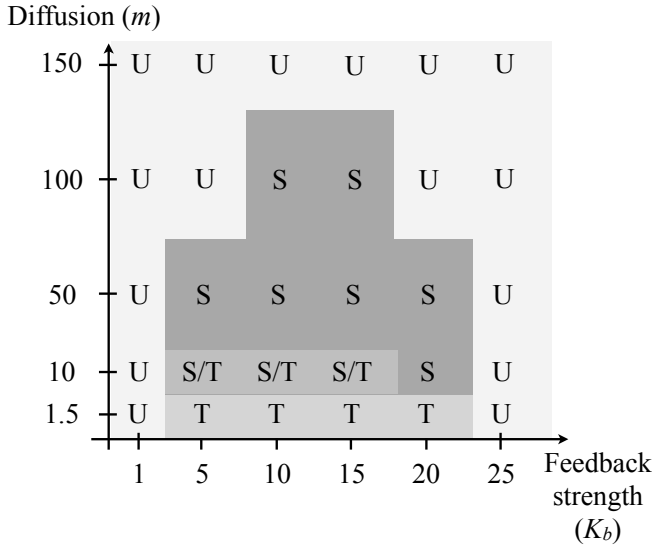

Figure 12. Model A: Steady states for different parameter combinations. The parameter values are shown in Table S2; letters indicate the steady states which are stable for a certain parameter combination, U - unpolarised, S - side polarised, T - triangular, S/T - bistable

the supplementary material. We find again that the unpolarised steady state, side polarity and the triangular state exist and are stable when they occur in the parameter scan. Similar to Model A, within the range of our choice of parameter values a low diffusion yields the triangular state while increasing the diffusion coefficients evokes a side polarised state in a direction determined by the initial condition. However, increasing the diffusion further by several orders of magnitude does not lead to the unpolarised state. For the unpolarised state the feedback strength has to be sufficiently high or sufficiently low and the diffusion sufficiently high. Choosing a slight initial vertex polarity we can show that the vertex polarised state exists but we could not detect a stable one. Figure 15 shows examples of the four different steady states.

This analysis gives strong evidence that for both models the vertex polarised state can exist, but when it does, it is always unstable. Due to the complexity of the models we cannot completely rule out the existence of a stable vertex polarised state. To ensure that this result is

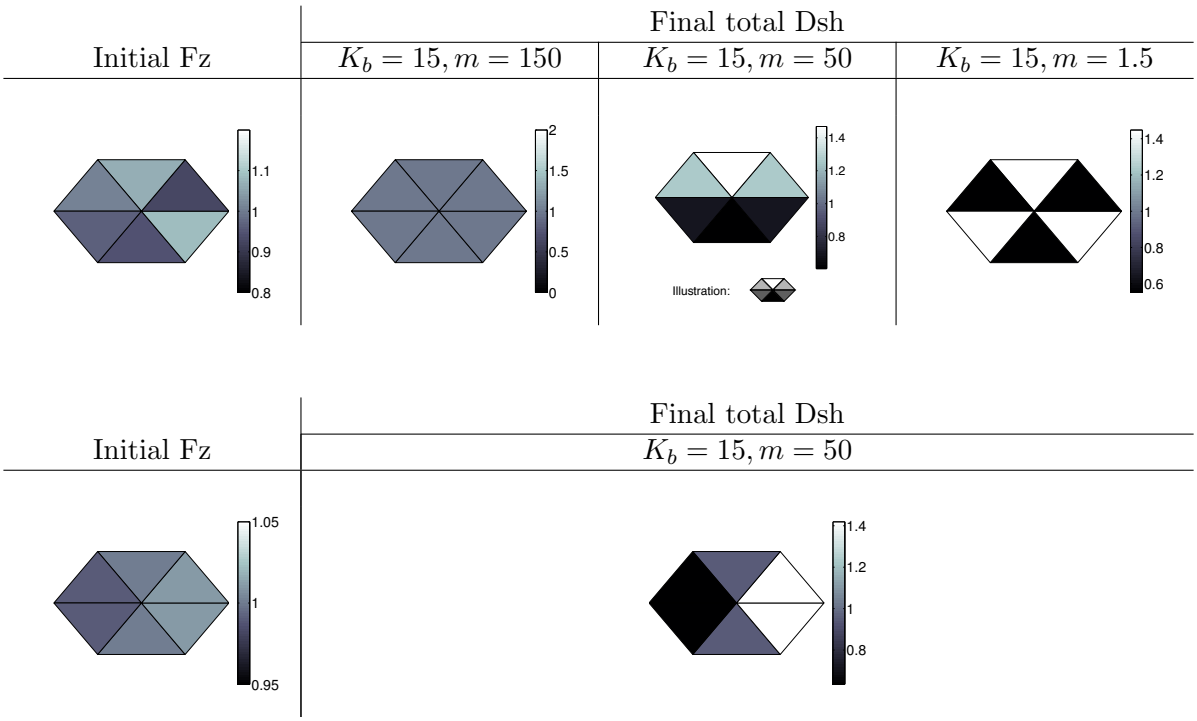

Figure 13. Examples of the steady states of Model A in a periodic array of hexagonal cells: top: inhomogeneous initial Fz distribution and final total Dsh distributions for a fixed feedback strength and different values of the diffusion coefficients. bottom: initial Fz distribution with a slight vertex polarity and final total Dsh distribution for a fixed feedback and diffusion strength. This state is not stable to pertubations. The remaining parameter values can be found in Table S2.

not an artefact of our discretisation we numerically approximated the solution of the full spatial models applying the finite element method. We considered different domains for the proteins that diffuse in the whole cell, proteins and complexes that only diffuse in the membrane and cell bridging complexes that are restricted to the edge of the membrane common to the cells they link together. We find that, for both models, a weak initial vertex polarity yields vertex polarity and a weak initial side polarity yields side polarity for the same parameter values, which agrees well with our findings so far, since it shows that vertex polarity is unstable to asymmetric perturbations (see supplementary material for more details).

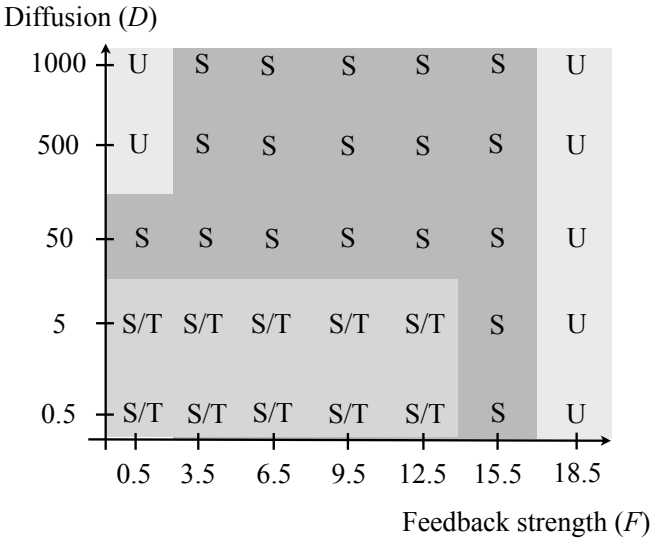

Figure 14. Model L: Steady states for different parameter combinations. Parameter values in Table S7; letters indicate the steady states which are stable for a certain parameter combination, U - unpolarised, S - side polarised, T - triangular, S/T-bistable; the values for the feedback strength were chosen to cover all possible behaviour.

Discussion

Planar cell polarity relies on the coordination of three modules: a global module that links the polarity of the individual cells to the tissue axis, a local module which ensures alignment

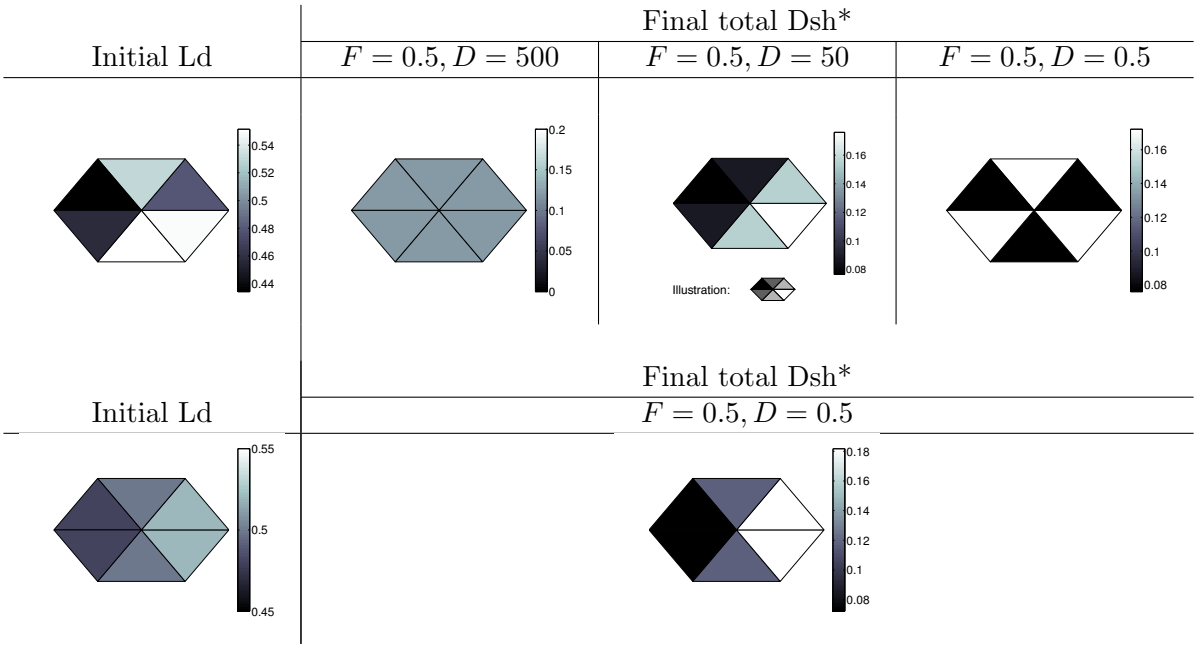

Figure 15. Examples of the steady states of Model L in a periodic array of hexagonal cells: top: inhomogeneous initial Ld distribution and final total Dsh* distributions for a fixed feedback strength and different values of the diffusion coefficients. bottom: initial Ld distribution with a slight vertex polarity and final total Dsh* distribution for a fixed feedback and diffusion strength. The remaining parameter values are presented in Table S7.

of neighbouring cells and a readout module that processes the polarity and ensures correct alignment of extracellular structures like hairs or bristles. To improve our understanding of how the first two modules could interact to establish planar cell polarity we conducted an analysis of Model A (adapted from [7]) and Model L (adapted from [8]). The two models share a similar logical structure and exhibit common behaviour. Both incorporate the global module as a persistent global cue which is read and amplified by feedback mechanisms involving the core proteins. For any parameter set, the global cue generates polarity which can be enhanced by the feedback mechanism. In the absence of a global cue the models yield a homogeneous unpolarised state or inhomogeneous polarised states depending on the parameter values and the initial conditions.

In one spatial dimension the inhomogeneous states are polarised to the right or the left, while in two spatial dimensions for hexagonal cells we obtain vertex polarity in six directions, side polarity in six directions or triangular states. In the absence of a persistent global cue, however, we find that vertex polarity in two dimensions is always unstable. Taken together these results show that to generate the type of distribution of the core PCP proteins observed in the developing *Drosophila* wing, with the two models that we have analysed, the persistent global cue is essential, while the feedback mechanisms act to amplify this cue and determine the strength of polarity.

One of the questions that arises from these results is whether nature uses a persistent global bias or a transient initial cue. If the latter is the case, our analysis predicts that the feedback mechanisms of the two models discussed here are insufficient. The feedback mechanism proposed by Burak and Shraiman [12] is more suitable as it can generate stable vertex polarity from a transient initial cue. From our understanding of the different models we conclude that the feedback mechanisms in Models A and L introduce a bistable switch across membranes of neighbouring cells, while the feedback mechanism proposed by Burak and Shraiman can generate tristability, which is essential to obtain stable vertex polarity in hexagonal cells. Considering our compartmentalised hexagonal cell, bistability ensures that states with different protein levels in

adjacent compartments are stable, i.e. side polarity and the triangular state. Tristability further enables the stability of states with a combination of adjacent compartments with the same protein level and adjacent compartments with different protein levels which is characteristic of a vertex polarised state (see Figure 11).

If nature uses a persistent global bias, the role of the feedback mechanism would be reduced to regulating the strength of polarity. In this case, the important question would be how the persistent global cue is implemented. In Models A and L the persistent global bias acts at two different levels. While Model A incorporates an intracellular persistent global cue (such that each cell is already polarised), Model L assumes a tissue-scale gradient. A variety of candidate mechanisms for the two alternatives have been proposed. The ligand gradient in Model L is based on the idea of a gradient of a putative 'Factor X', which is assumed to be a ligand for Fz but which has not been identified so far (reviewed in [13]). Another possibility is that the global module relies on the transmembrane proteins Dachsous (Ds) and Fat (Ft) and the cytoplasmic protein Four-Jointed, which are expressed in tissue wide gradients and interact to generate intracellular gradients, which might be read by the local module or the readout module (reviewed in [4]). Alternatively, work by Aigouy *et al.* [14] in the *Drosophila* wing suggests that the global cue is mechanical. They find that, due to the contraction of the hinge, wing cells are subject to anisotropic tension that regulates their alignment. An intracellular global cue could be generated by polarised transport along a polarised network of microtubules [15]. In addition to the cytoskeleton, the plasma membrane has been found to be involved in the polarisation of cells. In [16], Simons *et al.* show that the recruitment of Dsh by Fz and their interactions are dependent on the local pH and charge of the membrane.

This set of possible mechanisms for the global module has one common feature. They are all examples of a persistent global bias, indicating that this might be the mechanism generating long range coordinated polarity. It is still unknown, however, whether there is a "master" global cue that acts to orient all instances of downstream amplification mechanisms or whether multiple distinct cues have appeared during evolution and act independently. Judging by the variety of

possible mechanisms, the fruit fly might be too complex (or might rely on functionally redundant mechanisms) to address this question. Recent work has identified the involvement of the core proteins in cilia positioning in planarians [17]. Maybe such a simpler system could give more insight into the details of the global module.

A key question about the nature of the local module and its interaction with a global cue is whether or not the local module alone can generate stable long-range polarity from only a transient initial cue, as is the case for the feedback mechanism proposed by Burak and Shraiman [12]. Alternatively, it may be that the local module alone is capable only of aligning neighbouring cells and thereby determining the strength of polarity as in Models A and L. In this context, both the roles of the individual proteins within the feedback mechanism and the contribution of intracellular transport are essential. The parameter scans for the two-dimensional, compartmentalised versions of Model A and L show that for a transient initial cue the relative strengths of the feedback and the intracellular transport determine the final state (Figures 12 and 14). In particular, Model A yields only the homogeneous unpolarised steady state if the intracellular transport is increased above a certain level. This agrees with previous results from a more generic model of the local module [11].

To tackle these questions, we believe that future analysis of the system should aim at decoupling the global and the local module, preferably using a combination of theoretical and experimental approaches. Furthermore, it is important to investigate the interactions between the global, the local and the readout modules. Previously, it has been thought that the three act sequentially, such that the global cue is read and processed by the local module and the result is passed on to the readout module. However, several findings have challenged this view. In the abdomen the Ds/Ft system has been shown to polarise cells even in the absence of Fz [18], and in wings mutant for Pk the core proteins do not display an asymmetric distribution but the hairs grow at the right time and the right position [19]. Hence, it is likely that the interactions between modules are more complex. Possible scenarios would include the global module signalling directly to the readout module or to both the local and the readout module.

Acknowledgments

Author contributions

developed the theory: S. Fischer, P. Houston, N.A.M. Monk, M.R. Owen, performed the simulations: S. Fischer, wrote the paper: S. Fischer, N.A.M. Monk, M.R. Owen

References

1. Wang Y, Nathans J (2007) Tissue/planar cell polarity in vertebrates: new insights and new questions. Development 134: 647-658.

2. Guirao B, Meunier A, Mortaud S, et al (2010) Coupling between hydrodynamic forces and planar cell polarity orients mammalian motile cilia. Nature Cell Biol 12: 341-350.

3. Simons M, Mlodzik M (2008) Planar cell polarity signaling: From fly development to human disease. Annu Rev Genet 42: 517-540.

4. Axelrod JD (2009) Progress and challenges in understanding planar cell polarity signaling. Semin Cell Dev Biol 20: 964-971.

5. Tree DR, Ma D, Axelrod JD (2002) A three-tired mechanism for regulation of planar cell polarity. Sem Cell Dev Biol 13: 217-224.

6. Strutt D (2002) The asymmetric subcellular localisation of components of the planar polarity pathway. Cell Dev Biol 13: 225-231.

7. Amonlirdviman K, Khare NA, Tree DRP, Chen WS, Axelrod JD, et al. (2005) Mathematical modeling of planar cell polarity to understand domineering nonautonomy. Science 307: 423-426.

8. Le Garrec JF, Lopez P, Kerszberg M (2006) Establishment and maintenance of planar epithelial cell polarity by asymmetric cadherin bridges: A computer model. Dev Dyn 235: 235-246.

9. Raffard RL, Amonlirdviman K, Axelrod JD, Tomlin CJ (2008) An adjoint-based parameter identification algorithm applied to planar cell polarity signaling. IEEE Trans Autom Control 53: 109-121.

10. Le Garrec JF, Kerszberg M (2008) Modeling polarity buildup and cell fate decision in the fly eye: insight into the connection between the PCP and Notch pathways. Dev Genes Evol 218: 413-426.

11. Schamberg S, Houston P, Monk NAM, Owen MR (2010) Modelling and analysis of planar cell polarity. Bull of Math Biol 72: 645-680.

12. Burak Y, Shraiman BI (2009) Order and stochastic dynamics in Drosophila planar cell polarity. PLoS Comp Biol 5: 1-10.

13. Strutt D (2009) Gradients and the specification of planar polarity in the insect cuticle. Cold Spring Harb Perspect Biol 1: a000489.

14. Aigouy B, Farhadifar R, Staple DB, Sagner A, Röper JC, et al. (2010) Cell flow reorients the axis of planar polarity in the wing epithelium of drosophila. Cell 142: 773-786.

15. Shimada Y, Yonemura S, Ohkura H, Strutt D, Uemura T (2006) Polarized transport of Frizzled along the planar microtubule arrays in *Drosophila* wing epithelium. Dev Cell 10: 209-222.

16. Simons M, Gault WJ, Gotthardt D, Rohatgi R, Klein TJ, et al. (2009) Electrochemical cues regulate assembly of the Frizzled/Dishevelled complex at the plasma membrane during planar epithelial polarization. Nature Cell Biol 11: 286-294.

17. Almuedo-Castillo M, Saló E, Adell T (2011) Dishevelled is essential for neural connectivity and planar cell polarity in planarians. PNAS 108: 2813-2818.

18. Casal J, Lawrence PA, Struhl G (2006) Two separate molecular systems, Dachsous/Fat and Starry Night/Frizzled, act independently to confer planar cell polarity. Development 133: 4561-4572.

19. Strutt D, Strutt H (2007) Differential activities of the core planar polarity proteins during *Drosophila* wing patterning. Dev Biol 302: 181-194.